Some Noteworthy Aspects of the Hesston, Kansas, Tornado Family of 13 March 1990

Jonathan M. Davies,*
Charles A. Doswell III,+
Donald W. Burgess,**
and John F. Weaver++

Abstract

This paper considers a tornadic storm that struck south-central and eastern Kansas on 13 March 1990. Most of the devastation was associated with the first tornado from the storm as it passed through Hesston, Kansas. From the synoptic-scale and mesoscale viewpoints, the event was part of an outbreak of tornadoes on a day when the tornado threat was synoptically evident. Satellite imagery, combined with conventional data, suggest that the Hesston storm was affected by a preexisting, mesoscale outflow boundary laid down by morning storms. Radar and satellite data give clear indication of the supercellular character of the storm, despite limited radar data coverage.

Because of the considerable photographic coverage, several interesting features of the storm were recorded and are analyzed here. These include the following: 1) the movement and dissipation of a cloud band associated with an apparent rear-flank downdraft; 2) a transition from a rather large funnel through an apparent dissipation to the formation of a narrow funnel, during which the damage on the ground was continuous; and 3) a period of interaction between the first and second tornadoes.

1. Introduction

The afternoon and evening of 13 March 1990 witnessed an outbreak of at least 60 tornadoes in the central United States, from northwest Illinois to north Texas. This outbreak produced the strongest tornadoes on record for so early in the season that far north and west in the United States (*Storm Data,* March 1990). The outbreak included two unusually long-lived tornadic storms, one in northern Kansas and Nebraska and one in southern Kansas, each of which produced a tornado family. This paper will focus on the long-lived supercell storm event in south-central and eastern Kansas that produced a family of five tornadoes, including a violent tornado that struck the town of Hesston, north-northwest of Wichita, Kansas.

The Hesston supercell produced a family of at least five tornadoes, with a combined path of nearly 170 km (105 mi). The first three tornadoes in the series were particularly well documented photographically. With good visibility and timely warnings from the National Weather Service, several citizens were able to obtain excellent photographs and video recordings of the event from a number of vantage points. The resulting visual record provides an opportunity to examine some of the noteworthy events associated with the supercell and its attendant tornadoes, especially the most violent ones. This paper is concerned primarily with those noteworthy events.

Section 2 of this paper will summarize briefly the synoptic and mesoscale aspects of the situation. In section 3, a short overview of the supercell storm (henceforth called the Hesston supercell) that produced the tornadoes in south-central and eastern Kansas will be given. Some interesting features of the Hesston supercell storm and its tornadoes will be described in section 4, and a final discussion will be presented in section 5.

2. Synoptic and mesoscale environments

In general, the severe weather of 13 March 1990 fits the description "synoptically evident" (Doswell et al. 1993); that is, synoptic-scale structures favoring the development of severe convection are quite evident. The situation at 1200 UTC is a good match for a "type B" severe weather pattern (Miller 1972). This pattern is distinguished from Miller's "type A" pattern primarily by the presence of a major cyclone upstream of the event (as seen in Fig. 1). Convective available potential energy (CAPE) calculated from an interpolated sounding for the Hesston, Kansas, vicinity at 1200 UTC (Fig. 2) is about 3200 J kg^{-1}. This subjectively interpolated sounding is based primarily on the Topeka,

*Wichita, Kansas.
+NOAA/ERL National Severe Storms Laboratory, Norman, Oklahoma.
**NOAA/NWS Operational Support Facility, Norman, Oklahoma.
++NOAA/NESDIS—RAMM Branch, Fort Collins, Colorado.
Corresponding author address: Dr. Charles A. Doswell III, National Severe Storms Laboratory, 1313 Halley Circle, Norman, OK 73069.
In final form 8 March 1994.

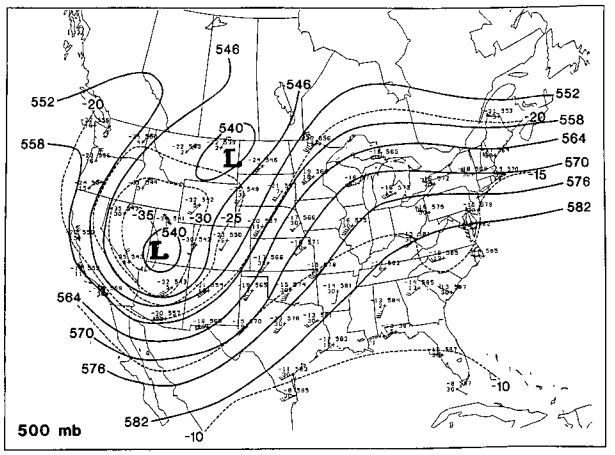

FIG. 1. The 500-mb analysis at 1200 UTC 13 March 1990, including geopotential height contours (dm, solid lines) and isotherms (°C, dashed lines), with conventional wind barbs (half-barb is 2.5 m s^{-1}, full barb is 5 m s^{-1}, and flag is 25 m s^{-1}).

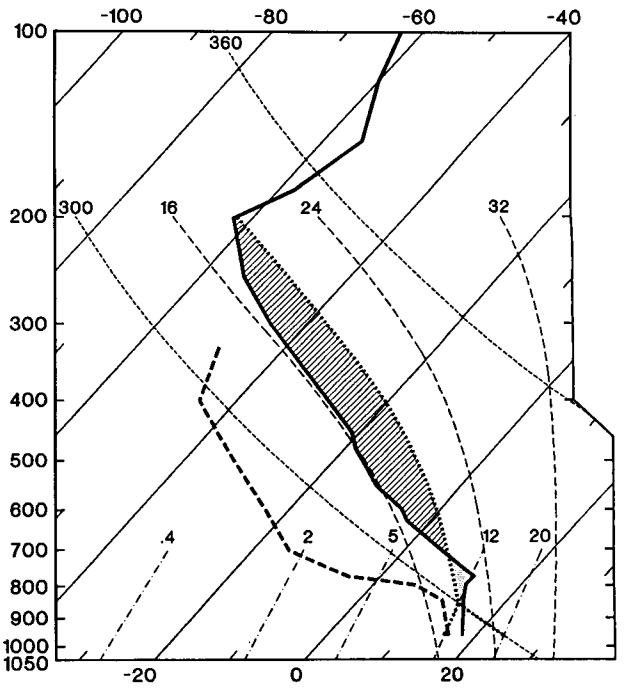

FIG. 2. Sounding interpolated for 1200 UTC, near Hesston, Kansas, on 13 March 1990, plotted on a skew T–log$p$ diagram; temperature trace is solid line, dewpoint trace is dashed line. The lifted parcel curve (dotted line) corresponds roughly to that of a parcel starting with the observed afternoon temperature of 24°C (75°F) and an average mixing ratio in the surface layer of 12 g kg^{-1}. Positive area is indicated by hatching, negative area by stippling.

Kansas, and Monett, Missouri, 1200 UTC soundings, modified at low levels with the surface data from near the time and location of the Hesston supercell, and through interpolations from the 850- and 700-mb analyses.

Further, there was considerable storm-relative environmental helicity (SREH) (Davies-Jones et al. 1990): an interpolated hodograph (shown in Fig. 3) for the Hesston vicinity at about 2100 UTC combined with an observed storm motion from 235° at 17 m s^{-1} (33 kt) has an SREH value of about 405 $m^2 s^{-2}$ (for the layer from the surface to 3 km). The subjective hodograph interpolation is based primarily on the Topeka, Kansas, and Monett, Missouri, 0000 UTC wind profiles, again modified slightly at low levels using the surface analyses and interpolations from the low-level constant pressure charts.

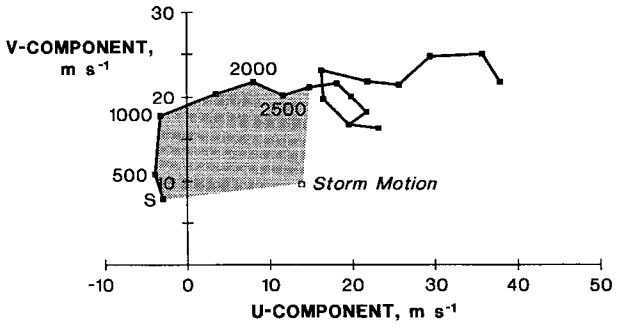

FIG. 3. Hodograph interpolated to near Hesston, Kansas, at about 2100 UTC, showing the storm motion (from 235° at 17 m s^{-1}). The area indicative of the surface (S) to 3-km storm-relative helicity is stippled; axes are in m s^{-1}. Squares on the hodograph are at 500-m intervals.

Although CAPE and storm-relative helicity parameters do not constitute a comprehensive analysis of the synoptic situation, they certainly suggest that the pattern favored development of supercells; the CAPE and helicity are within the range suggested by Johns et al. (1993) as favorable for supercells that may produce strong and violent tornadoes.

During the previous evening, and on into the early morning hours of 13 March, convection had developed in Oklahoma and moved relatively rapidly northeastward across Kansas and into Iowa and Illinois by 1200 UTC. Additional convection developed during the morning in the warm sector of the large-scale weather system, south of a quasi-stationary front that lay across northwestern Kansas, and east of a dryline that intersected the front (Fig. 4). This convection moved across central and eastern Kansas by late morning, leaving behind an outflow boundary. The best evidence for this boundary is in the satellite imagery, where it is delineated by cloud lines and a change in character of the low-level clouds (e.g., Fig. 5); the sparsely distributed surface observations give little hint of this mesoscale feature.

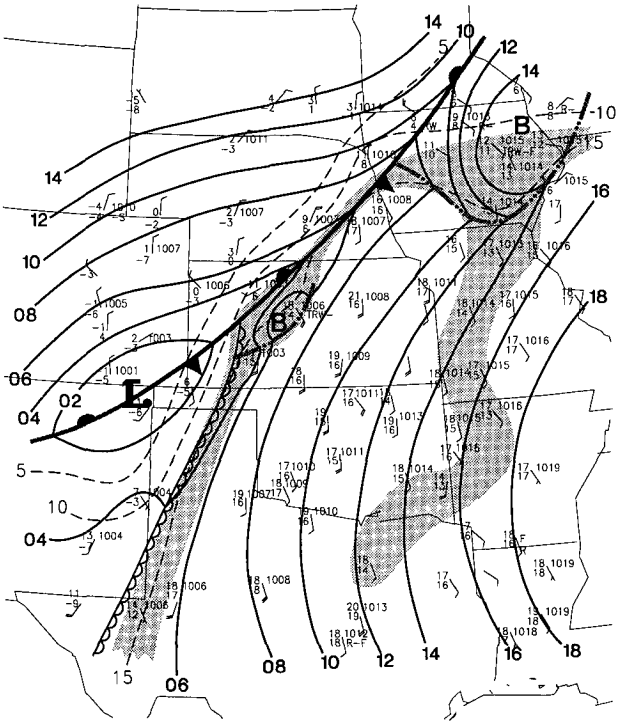

FIG. 4. Surface analysis at 1200 UTC on 13 March 1990. Isobars (mb) are solid lines, isotherms (°C) are dashed lines, the stippling denotes dewpoint temperatures between 10° and 15°C (inclusive), and frontal symbols are conventional, while light, dash–double dot lines depict outflow boundaries, and "B" denotes a "bubble" or mesohigh. Station plots and wind barbs are conventional.

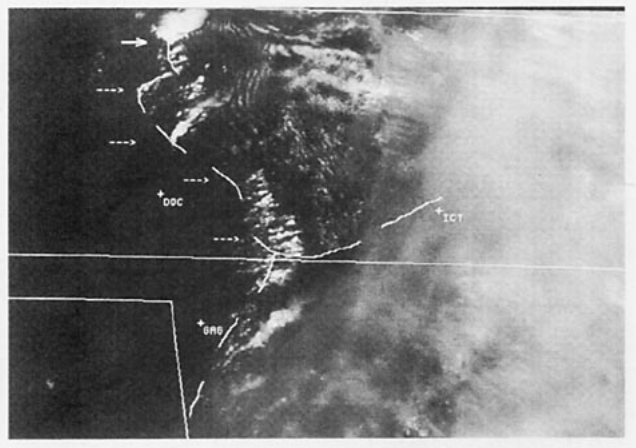

FIG. 5. Visible satellite image at 2001 UTC on 13 March 1990. Dodge City, Kansas (DDC), and Gage, Oklahoma (GAG), are indicated with plus signs, and dashed arrows point to a cumulus cloud line along the western edge of the mesoscale outflow boundary. Most of central and eastern Kansas are covered with anvil cirrus. The solid arrow indicates the complex that developed into the northern Kansas–Nebraska supercell.

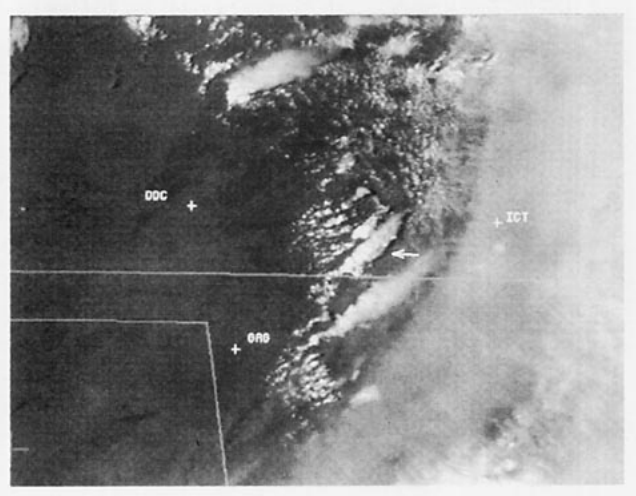

FIG. 6. As in Fig. 5 except at 2046 UTC. The arrow indicates the developing convection that would become the Hesston supercell.

3. The Hesston supercell

During the afternoon, the mesoscale outflow boundary from the morning activity began to erode along its western edge (Fig. 5), perhaps due to strong westerly winds. Over west-central Kansas, a complex of congestus and a developing cumulonimbus formed at the point where the boundary curved back toward the northeast. This complex went on to develop into the supercell that produced the Nebraska tornadoes. Meanwhile, the mesoscale outflow boundary in south-central Kansas remained in place.

The convective towers that would grow into the Hesston storm began in extreme southern Kansas near 2000 UTC and first produced a cirrus anvil in the visible satellite imagery at 2046 UTC (Fig. 6). The first radar echo was observed at nearly that time about 160 km (100 mi) southwest of Hesston. Initially, the storm was weak and multicellular; several updrafts occurred simultaneously along a southwest-to-northeast line. As vigorous new updraft towers formed on the upwind (southwest) flank of the storm, intensification began, with the first 50-dB*Z* core observed at 2130 UTC. At this time, the storm began to move northeastward, along the mesoscale boundary.

By 2215 UTC, the storm showed evidence of becoming severe, with strong convective towers on the right-rear storm flank (relative to storm motion) and an associated arcus cloud band indicative of a low-level outflow boundary (Fig. 7). Although the limited available radar data (not shown) are not sufficient to reveal structural details [including features that might *confirm* supercell characteristics, such as a bounded weak echo region (BWER)], the echo's large size and elliptical shape suggest that it might have been undergoing a transition to supercell status (Lemon 1980) at about this time.

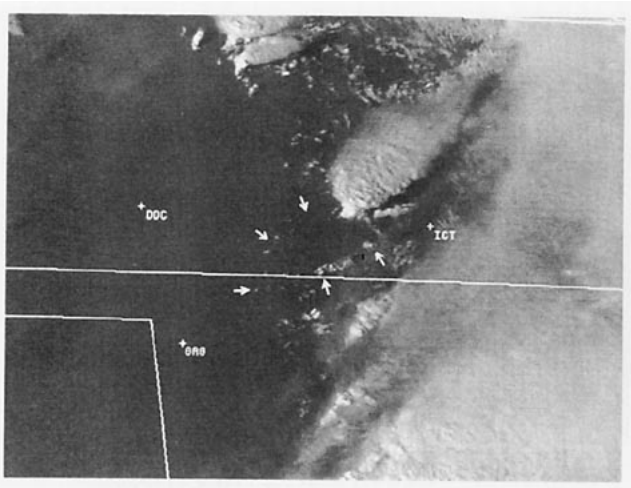

FIG. 7. As in Fig. 5 except at 2216 UTC. The arrows point out clouds forming a ring about what is apparently a newly created outflow boundary. Wichita, Kansas, is indicated with a plus sign.

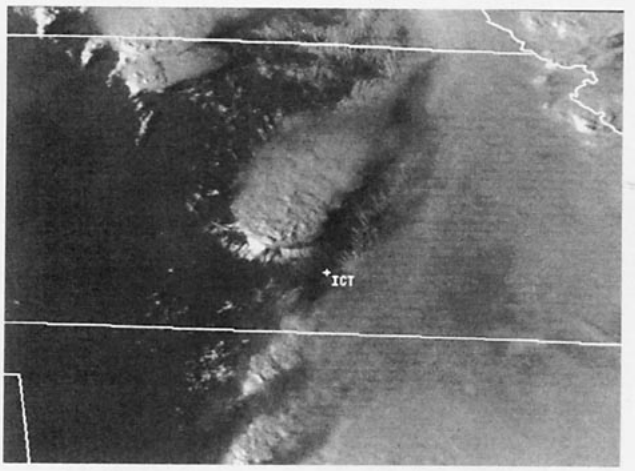

FIG. 8. As in Fig. 7 except at 2231 UTC. Note the rapid development of the cumulus clouds east and west of the convective towers forming the Hesston storm to the west-northwest of ICT (see text).

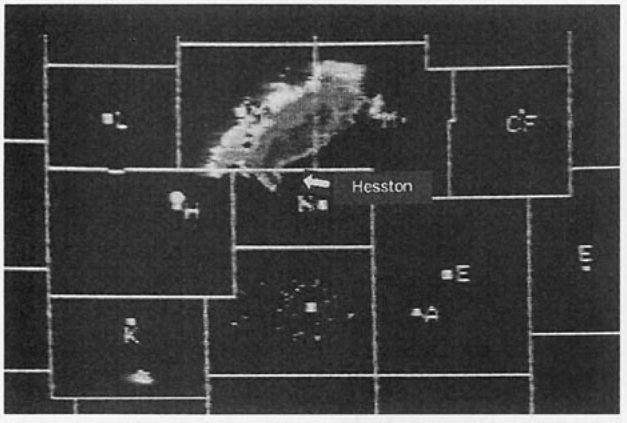

FIG. 9. Radar image (courtesy of KAKE-TV, Wichita, Kansas) at about 2315 UTC. Shading shows different reflectivity levels (calibration unknown); Hesston's location is indicated by the arrow; "N" denotes Newton, Kansas; "H" denotes Hutchinson, Kansas; "M" denotes Marion, Kansas; "CF" denotes Cottonwood Falls, Kansas; "L" denotes Lyons, Kansas, and the unlabeled mark with scattered spots surrounding it is the KAKE-TV radar site in Wichita, Kansas.

FIG. 10. Ground-based photograph, showing the storm shortly before 2315 UTC. (Photograph by D. Nelson.)

Between 2216 and 2231 UTC, shortly before the first tornado (at 2234 UTC), a set of short, evenly spaced lines of cumulus appeared on either side of the supercell's convective tower and orthogonal to the outflow boundary (Fig. 8). Sequential imagery shows that the ends of these cloud lines were moving westward relative to the storm, suggesting a secondary surge of outflow. These regularly spaced cumulus lines have been observed occasionally in the past by National Environmental Satellite Data and Information Service (NESDIS) meteorologists, in association with tornadic storms, but their origins are not known.

By 2315 UTC, the satellite and radar imagery give clear indication that the storm was a supercell. The overshooting top of the storm was located near Hesston and the tornado-bearing right flank was southwest of the town. The anvil had expanded northeastward to a point beyond the Nebraska border, indicating strong storm-top divergence and fast jet stream winds. The radar echo (Fig. 9) depicted a hook-shaped echo indicative of supercell character (Forbes 1981) as the storm approached Hesston.

A photograph made somewhat before 2315 UTC relates the ground-based visual appearance of the storm to other perspectives (Fig. 10). The photo was taken from just west of Hesston, looking southwest; the tornado is visible at the southwest edge of the main convective tower (that beneath the overshooting top). Rotating rain curtains that compose the hook echo are discernible on the far side of the convective tower and tornado. Note the prominent low-cloud band to the right (northeast) of the tower. This band may be associated with the boundary between the forward-flank downdraft (rain cooled) air and the unmodified inflow. It also might be related to the mesoscale outflow

boundary left behind by earlier convective storms (as discussed above), since it extended for some distance along the storm's right flank. Unfortunately, this conjecture cannot be validated, owing to that part of the storm being covered by its anvil. The laminar character of this cloud band suggests it arose from forced lifting that did not reach the level of free convection. This implies (but does not confirm) the presence of a low-level stable layer capping the warm, moist inflow and acting to limit the development of nearby convection that would compete with the main storm.

4. The Hesston tornado

Figure 11 provides an overview of the entire tornado outbreak, as well as major city locations for orientation purposes. The Hesston supercell produced five tornadoes (according the a survey by the University of Chicago), the first of which was the one to hit Hesston. A second significant tornado, passing near the city of Goessel, Kansas (and hereinafter referred to as the "Goessel tornado"), interacted with the Hesston tornado during the latter stages of its life. The third, fourth, and fifth tornadoes passed mostly over open country, including the Flint Hills region of Kansas, producing little significant damage.

Our assessment of the noteworthy features produced by the Hesston tornado is based mostly on some simple photogrammetry of the available video and sets of still photographs collected after the storm. One of us (JMD) conducted an extensive ground survey of the Hesston area, making measurements from the photograph and video locations to provide a basis for the photogrammetry. A summary of the methods involved can be found in Holle (1986). We have estimated that our measurements have an imprecision of about 15%.

a. A cloud band

During the early stages of the life cycle of tornado 1, the nearly simultaneous photographs by J. Davies and K. Smith suggested that we might be able to track the movement of an interesting cloud band that apparently was rotating around the tornado/wall cloud. Unfortunately, the positions of the two photographers do not permit a reliable quantitative determination because the tornado is very nearly along the line connecting the two observers and the photographic evidence does not include any landmarks common to the photographs of the two photographers. This precludes quantitative analysis, but we offer the following *qualitative* analysis based on the images of K. Smith.

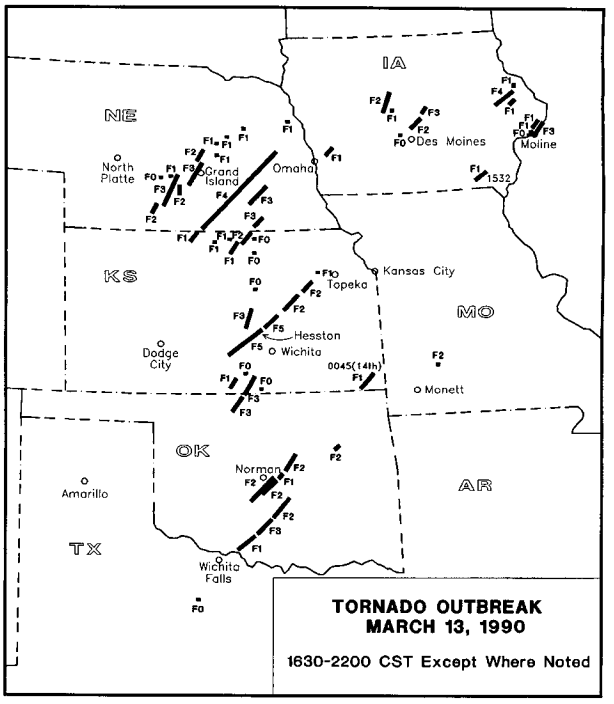

FIG. 11. Map of the overall outbreak, showing major place locations.

During a postevent survey, azimuths to landmarks in the photographs were obtained and used to determine azimuth angles across the photographs. By using the known tornado track, and by assuming that the axis of the visible funnel was approximately in the center of the path, distance estimates to the tornado could be made. From these estimates, and knowing the time between photographs, the speed of tornado movement during this period is about 17 m s^{-1}. Although there is no way to fix the locations along the cloud band shown in Fig. 12, the azimuths to various

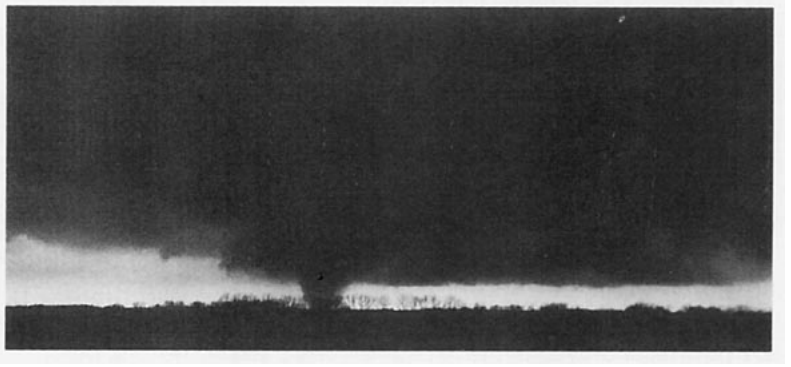

FIG. 12. Photograph of the cloud band (extending to the right of the tornado) at about 2237 UTC. (Photograph by K. Smith, corresponding to No. 8 on Fig. 13.)

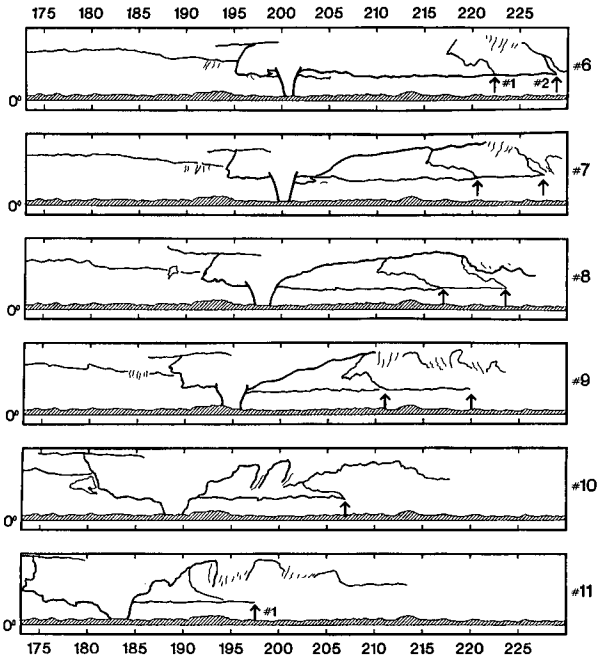

FIG. 13. Series of tracings of pertinent features along the cloud band as it evolves in time; numbers to the right correspond to photograph numbers in the sequence taken by K. Smith, with No. 9 taken at about 2238 UTC. Arrows locate the ends of the bands (Nos. 1 and 2) tracked in Table 2. Time separation between images is given in Table 2.

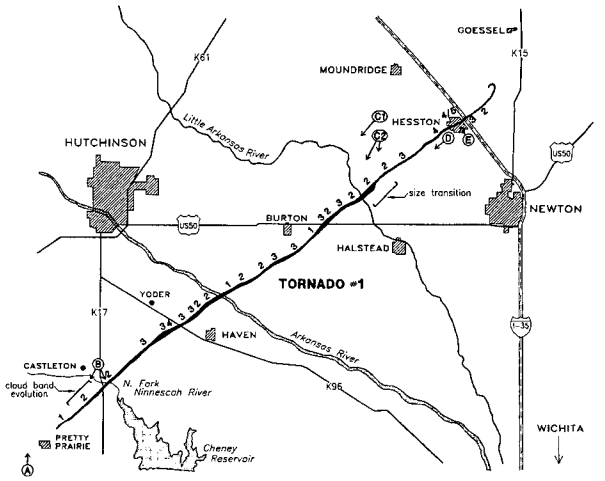

FIG. 14. Detailed map of the track for tornado 1. Photographer locations are shown by the circled letters (**A:** J. Davies; **B:** K. Smith; **C1** and **C2:** D. Nelson; **D:** C. Berry and D. Graham; and **E:** D. Alison) (see Table 1 for further details), with arrows indicating roughly the direction toward which the photographs were taken. Numbers shown along the tracks are F-scale ratings assigned by the University of Chicago. Indicated along the path are the locations of the cloud band evolution and funnel size transition described in section 4.

features on the photographs can be estimated from the azimuth-annotated photographs (see the calibrated tracings in Fig. 13) if the distance to the features is assumed to be about the same as the distance to the tornado (although there is no reason to believe that this is quantitatively correct). From these calculations, the average speed of band 1's movement is 10.5 m s^{-1}, whereas that for band 2 is similar: 9.7 m s^{-1}. Results of the photogrammetry are summarized in Table 2. Recall that all values are only accurate to within roughly 15%, but the *relative* changes may be somewhat more reliable than that.

Simply inspecting the photographs reveals that the cloud band's angular separation from the tornado is decreasing, apparently the result of cloud dissipation in response to an intensifying rear-flank downdraft (to the right of the tornado in the figures). If the movement of the cloud bands is, therefore, considered to be a contribution to the tornado-relative flow contributed by the rear-flank downdraft, then this might act to increase the tangential flow speed as the downdraft wraps around the tornado. Therefore, it is interesting to note that shortly after these pictures were taken, the tornado increased in both size and intensity, based on the damage assessments. It is possible that the evolution of the cloud band was a precursor to this increase in tornado size and strength, although such a conjecture cannot be validated with the available information.

b. A size transition

Later in the life of tornado 1, as it continued to approach Hesston, three photographers (D. Nelson, D. Graham, and C. F. Berry) were photographing the tornado from different locations (see Fig. 14 and Table 1) at nearly the same times during a size transition phase. This permitted some photogrammetric estimates of the change in funnel cloud diameter during the transition. Although the photographers were not necessarily ideally positioned for photogrammetry (i.e., at large angular separation), the geometry does permit reasonably reliable computations.

Photogrammetry results are summarized in Table 3. There are certain difficulties associated with this calculation since the width of the funnel cloud is notnecessarily the same as the width of the damage path, and the horizon obscures the lower portion of some of the Berry photographs. Note that with two photographers, it is possible to compute widths in three different ways: 1) use the image of photographer 1 for single-camera photogrammetry based on the angular width of the subject and its distance from the photographer, 2) use the image of photographer 2 in the same single-camera mode, or 3) use both photographer's images to find the

intersections of the rays defined by the subject's edges. The first two methods will tend to underestimate the diameter slightly, while the third method will tend to overestimate the diameter slightly. In the actual measurements it can be shown that the errors associated with these effects are quite negligible.

With the above caveats in mind, we make the following analysis of the results. During the wide phase, the funnel was roughly 440 m wide at the near-ground level (Fig. 15). As the funnel underwent apparent dissipation, the debris "cloud" remained large (about 550 m, Fig. 16a). Later in the transition, a funnel appeared in the interior of the debris cloud (Fig. 16b), the latter of which had a diameter of about 515 m. Finally, with the transition complete, the funnel was roughly 60 m wide at the ground (Fig. 16c).

Given the evolution we have just described, an implicit issue concerns whether or not the observed process actually represents the dissipation of the tornado, followed by its "replacement" by another, separate tornado. In this particular case, it appears that the damage track is continuous and the disappearance of the condensation funnel does not constitute a dissipation of the tornado. Nevertheless, since the tornado funnel is not an *object* but a visible manifestation of a *process,* it must be continually renewing itself. Is a temporary lull in the renewal process(es) sufficient to mark the "end" of the tornado or simply a fluctuation in intensity? In this case, the continuity of damage makes the issue clear, but it is not hard to imagine a more ambiguous situation, as in a tornado over open country with little to depict the changing intensity. As we learn more about tornadoes, and atmospheric vortices in general, these rather subtle issues become more apparent. The decisions made in any particular event *do* affect such topics as tornado climatology, so they should not be made in ignorance; unfortunately, we typically do not have sufficient evidence even to ask the right questions, much less to provide unambiguous answers.

c. An interaction between the Hesston and Goessel tornadoes

Finally, as tornado 1 was shrinking and dissipating, tornado 2 was developing nearby (approximately 1.5

TABLE 1. Photo (P) and video (V) contributors, in approximate chronological order, with location information (all towns are in Kansas).

Contributor(s)	Location information
Jon Davies (P)	2–3 mi S of Sawyer, looking S. Also, 4 mi N, 1/2 mi E of Kingman, looking NNE. Also, 1 1/2 mi S of Pretty Prairie to N edge of Pretty Prairie, looking NNE
Ken Smith (P)	1 mi E of Castleton, 1/2 mi W of Hwy K-17, looking SW through SE
Doug Nelson (P)	5 mi W of Hesston, looking SW. Also, 5 mi W, 1 1/2 mi S of Hesston, looking SW through S. Also, 5 mi E, 4 mi N of Hesston (3 mi S of Goessel), looking N
Chuck (C.F.) Berry (P) and Duane Graham (P)	SW edge of Hesston, looking SW
Bill and Nancy Hugie (V)	W edge of Hesston, looking SW
Dean Alison (V)	1 mi SE of Hesston, looking NW
Peg Wieland (P)	N-central Hesston, looking NE
Wendell Mains (P)	NE edge of Hesston, looking NE
Beth Eason and Bobbie Harris (P)	2 mi E of Hesston, looking WNW
Nelson Dreier (V)	2 1/2 mi E of Hesston, looking W through NNE
Nancy Franzen (P)	6 mi E, 2 1/4 mi N of Hesston, looking WSW through WNW
Olin and E. T. Harris (V)	5 mi E, 2 1/2 mi N of Hesston, looking WSW through N
Mike Schmidt (V)	3 mi S of Goessel, looking SSW
Denise Bina (P)	1 mi E, 2 1/2 mi N of Pilsen, looking SW through NE

TABLE 2. Results of photogrammetric analysis of the mesocyclone-associated cloud band, showing computed speed of band-end motion, assuming the band end is at the same distance as the average distance to the tornado during the interval between pictures. The two different band ends are identified with arrows in Fig. 13.

Picture interval	Band end 1 (m s^{-1})	Band end 2 (m s^{-1})	Time (s)	Avg. distance (km)
6–7	8.5	5.6	15	4.86
7–8	15.1	13.5	24	4.62
8–9	11.7	8.5	35	4.26
9–10	4.9	—	53	3.72
10–11	14.3	—	39	3.19

TABLE 3. Results of photogrammetric analysis of the funnel width transition. All photographs shown in the figure referenced are by D. Nelson. The "ray intersection" method refers to two-camera measurements, while the other measurements are done with the single-camera method. Width measurements are in meters, with "suggested estimate" arrived at subjectively during the analysis.

Description of measurement	Photograph(s)	Width (m)	Comments
Wide phase (Fig. 15)			
Funnel, midlevel	Nelson	814	
	Berry	880	
	Ray intersection	864	
	Suggested estimate	870	
Funnel, ground level	Nelson	398	
	Berry	469	
	Ray intersection	456	
	Suggested estimate	442	
Dissipation phase (Fig. 16a)			
Debris cloud, ground level	Nelson	546	No visible funnel cloud
	Berry	551	
	Suggested estimate	548	
New funnel phase (Fig. 16b)			
Debris cloud, ground level	Nelson	512	
	Graham	515	
	Suggested estimate	514	
Interior funnel, midlevel	Nelson	107	Obscured at ground level by larger debris cloud
	Graham	103	
	Suggested estimate	105	
Subsidiary cloud length	Nelson	274	Subsidiary cloud on north side of interior funnel
	Graham	247	
	Suggested estimate	259	
Complete transition (Fig. 16c)			
Funnel, cloud base	Nelson	228	Only usable photograph
Funnel, ground-level	Nelson	66	
	Berry	47	
	Suggested estimate	61	

km) just after 2335 UTC (Fig. 17). From 2335 to 2340 UTC, tornado 1 shrank rapidly as tornado 2 increased in size, and Fujita (1992, p. 45) has suggested that the two tornadoes rotated about a common center during this phase. Fujita's analysis of the photographic evidence (Fig. 18) reveals that the dissipating tornado 1 rotated around the developing tornado 2, disappearing from the photographs shortly after 2340 UTC.

Although it is not entirely clear how to specify the location of Fujita's proposed common center, it is equally clear that the two vortices interacted strongly for these several minutes. One gets the visual impression of a diminution of the circulation about tornado 1, accompanied by a concomitant enhancement of the circulation about tornado 2, so that the path of tornado 1 on the ground is more heavily affected by the circulation of tornado 2 than vice versa, especially toward the end of the interaction. It is also interesting that tornado 1 deviates from its essentially straight track just prior to the interaction and that tornado 2 apparently continues along the extension of that same path after the interaction is complete. It is possible that for reasons that are not entirely clear (perhaps a nearby microburst or an intensification of the rear-flank downdraft, as discussed above), tornado 1 is "pushed" out of the center of the mesocyclone. The development of tornado 2 is also apparently not at the mesocyclone center, so in effect the two tornadoes are, for a time, subvortices within the mesocyclone. The completion of the interaction is signaled by the relocation of the primary vortex (number 2) near the mesocyclone center, which is accompanied by a rapid intensification to violent intensity.

Overall, the interaction appears similar to that described by Lander and Holland (1993) for tropical cyclones. They assert that "merger does not follow the classical binary vortex model of coalescence at the centroid. Rather, one cyclone tends to lose its convective forcing and become sheared into the circulation of the other." This description matches the interaction between the Hesston and Goessel tornadoes rather well.

As a final note on this occurrence, Fujita (1992) has called attention to another famous pair of vortices: those near Midway, Indiana, on the day of the so-called Palm Sunday tornado outbreak of 11 April 1965 (see Fujita et al. 1970). It appears that in that case as well, two vortices in close proximity interacted strongly,

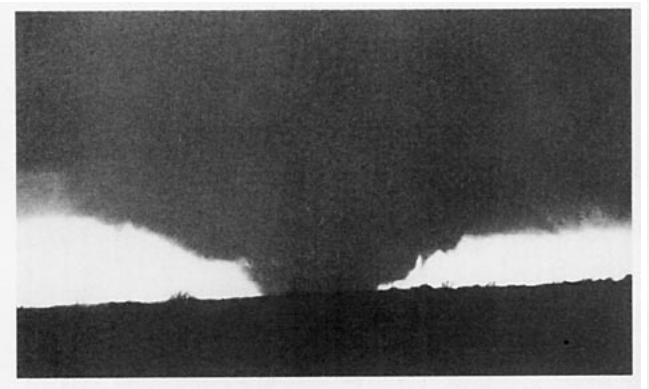

FIG. 15. Wide condensation funnel at about 2319 UTC. (Photograph by D. Nelson.)

with one dissipating and the other developing and continuing (see Fig. 46 in Fujita et al. 1970). Apparently, the interaction on 11 April 1965 was more rapid, with the two vortices being closer initially than on 13 March 1990.

5. Discussion

It appears that the preexisting mesoscale outflow boundary played an important role in the evolution of the event (see Maddox et al. 1980). Also, the sudden appearance of cumulus cloud lines prior to the tornado is an intriguing observation that deserves further attention. Additional interesting aspects of the storm were those details revealed by the relatively abundant storm and tornado photography/videos. Both the size transition and the interaction between the first and second tornadoes illustrate some of the problems associated with defining tornadic events. That is, although the damage on the ground can be quasi-continuous, deciding whether or not visible vortices constitute separate tornado events can become subtle and confusing. This is a problem that will not simply go away with better information, because atmospheric vortices are complex and challenging subjects for study. In a sense, the more information we have, the more confusing and problematic the events become. As we move into an era with better radar coverage than ever before, including Doppler capability, users of those data need to be prepared for the challenges, as well as the opportunities, offered by the enhanced data.

Given the proliferation of inexpensive, simple video cameras, it is increasing likely that at least some video images will be obtained for many, if not most, significant tornado events. Moreover, it is possible that future field studies of tornadoes and tornadic storms will use film and/or video documentation of the

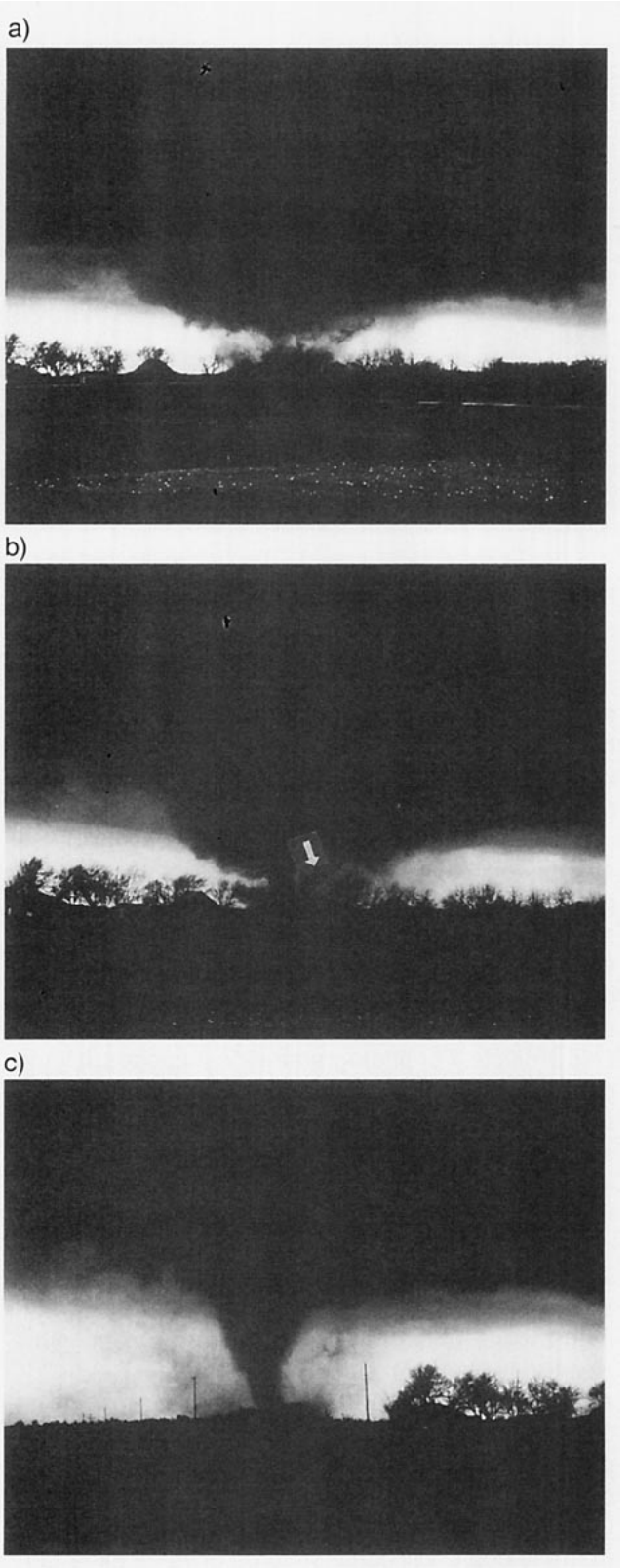

FIG. 16. Funnel width transition photographs, including superposed annotations: the wide phase is seen in Fig. 15 at 2319 UTC, followed by (a) funnel dissipation phase at 2322 UTC, (b) interior funnel redevelopment phase at 2323 UTC showing the "subsidiary cloud" on the north side of the funnel (arrow), and (c) completed transition phase at 2324 UTC. Times are approximate, based on Hugie video's internal clock time. (Photographs by D. Nelson.)

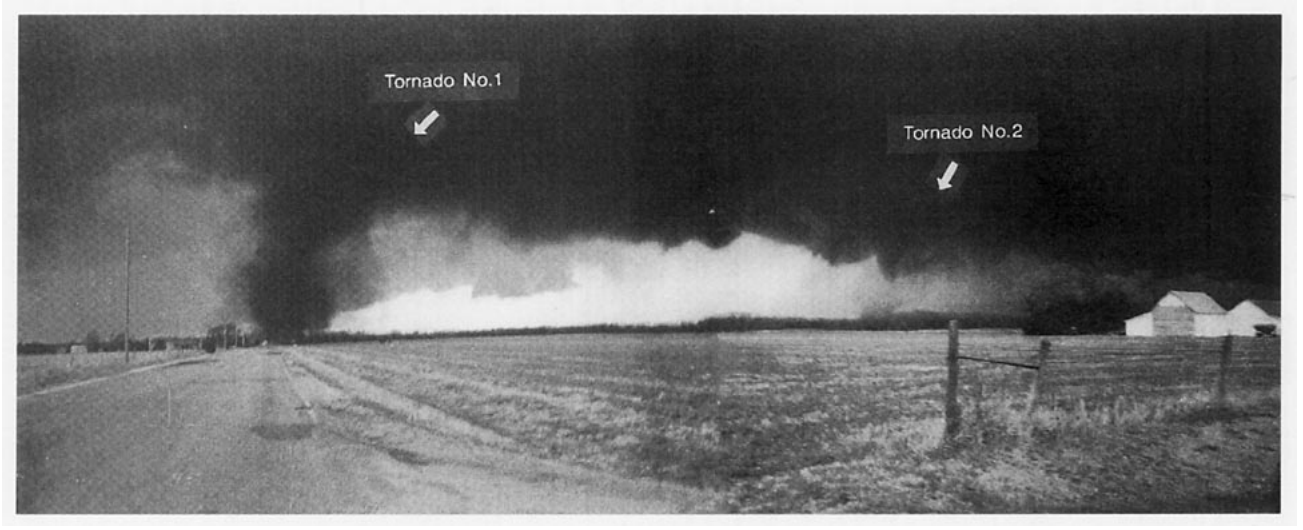

FIG. 17. Photograph of developing tornado 2 at about 2338 UTC as tornado 1 moves out of Hesston. (Photograph by B. Harris and B. Eason.)

events. Photogrammetric analysis could (and should) become reestablished as an important tool in trying to map the flow fields within tornadoes and tornadic storms. However, although videos obtained from the untrained public can be helpful in studying these events, it is obvious that people do not always take positions to maximize the quality of photogrammetric analysis. Substantial effort is needed to obtain the most useful imagery for analysis, and we have indicated some of the problem areas that will need attention in scientifically designed photogrammetry field projects. For photogrammetric purposes, it turns out that 16-mm movie film continues to have superior resolution. Even the so-called high-end, most expensive video cameras have only about one-third of the linear resolution of 16-mm film. The latter corresponds to about 1000 lines per inch, whereas high-quality consumer video cameras employ about 350 lines per inch. The least expensive consumer videos have even less resolution. Therefore, for scientific photogrammetric work, 16 mm is still preferred over video, but it is unlikely that the public will ever use the bulky, expensive 16-mm cameras. Still photographs using 35-mm cameras typically are of excellent quality for photogrammetry, assuming exposure and focus are done properly, but have severe limitations for rapidly changing subjects like tornadoes. Still photographs from the public will continue to be of value for larger-scale subjects that are not fast changing. Although videos provided by the public cannot replace coordinated field efforts to obtain high-quality photogrammetry data, they can provide a valuable *supplemental* source of quantitative information about tornadoes and storms, if they are analyzed.

Finally, we wish to stress the need for immediate deployment of survey teams after significant events. Since cleanup commences rapidly after such a storm, speed of deployment is essential. Engineering analysts should be regular participants in such fast-response surveys, before the important information is lost during cleanup. Both aerial and ground surveys must be done, as the insights from one are important for understanding the other. If we are to learn from these tragic events, we must be ready to obtain the needed information quickly and efficiently. It is unfortunate that at a time when our technological capabilities are growing more rapidly than ever before, and when expanding urban areas make it ever more likely that tornadic storms will create disasters, we are scaling back on the resources for obtaining critical

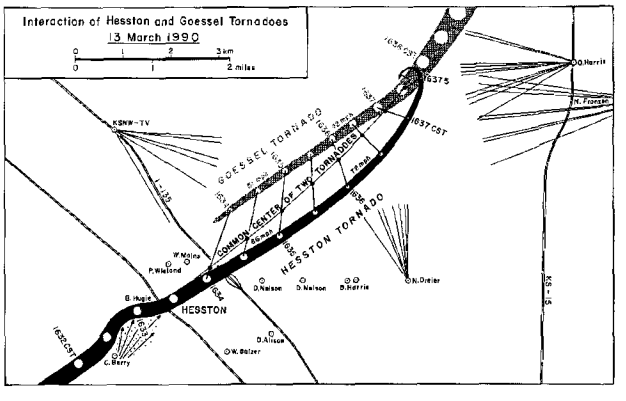

FIG. 18. Fujita's analysis (from Fujita 1992, with permission of the author) of the interaction phase between tornado 1 (the "Hesston" tornado) and tornado 2 (the "Goessel" tornado).

information and for doing the research needed to learn the important lessons from such events.

Acknowledgments. We wish to thank those who supplied video, photographs, and descriptions: Dean Alison, C. F. Berry, Nelson Dreier, Duane Graham, Bill and Nancy Hugie, Wendell Mains, and Peggy Wieland of Hesston, Kansas; Nancy Franzen, E. T. Harris, Mike Schmidt, and Roland Funk of rural Newton, Kansas; Beth Eason and Bobbie Harris of Peabody, Kansas; Ken Smith of Wichita, Kansas; Doug Nelson of Centralia, Kansas; Olin Harris of Walton, Kansas; and Denise Bina of Lincolnville, Kansas. Various individuals contributed by helping us to obtain data used in the analysis, including Rob White, Dave Schaffer, Bob Johns, Stan Reimer, Roy Britt, Ted Fujita, Duane Stiegler, Grant Goodge, Fred Carr, Dan Spaeth, Tim Marshall, Gene Rhoden, and Bobby Prentice. We thank Prof. Fujita for permission to use his figure (our Fig. 18). Drs. Erik Rasmussen and Harold Brooks offered useful criticisms of an earlier version of the manuscript, and Dr. J. F. W. Purdom provided useful input to the interpretation of the satellite images. Ms. Joan O'Bannon assisted with figure preparation.

References

Davies-Jones, R., D. Burgess, and M. Foster, 1990: Test of helicity as a tornado forecast parameter. Preprints, *16th Conf. on Severe Local Storms,* Kananaskis Park, Alberta, Canada, Amer. Meteor. Soc., 588–592.

Doswell, C. A., III, S. J. Weiss, and R. H. Johns, 1993: Tornado forecasting: A review. *The Tornado: Its Structure, Dynamics, Prediction, and Hazards, AGU Geophys. Monogr.,* No. 79, Amer. Geophys. Union, 557–571.

Forbes, G. S., 1981: On the reliability of hook echoes as tornado indicators. *Mon. Wea. Rev.,* **109,** 1457–1466.

Fujita, T. T., 1992: *Memoirs of an Effort to Unlock the Mystery of Severe Storms During the 50 Years, 1942–1992.* University of Chicago, 298 pp.

——, D. L. Bradbury, and C. F. Van Thullenar, 1970: Palm Sunday tornadoes of April 11, 1965. *Mon. Wea. Rev.,* **98,** 29–69.

Holle, R. L., 1986: Photogrammetry of thunderstorms. Vol. 3, *Thunderstorms: A Social and Technological Documentary,* 2d ed., E. Kessler, Ed., University of Oklahoma Press, 77–98.

Johns, R. H., J. M. Davies, and P. W. Leftwich, 1993: Some wind and instability parameters associated with strong and violent tornadoes. Part II: Variations in the combinations of wind and instability parameters. *The Tornado: Its Structure, Dynamics, Prediction, and Hazards, AGU Geophys. Monogr.,* No. 79, Amer. Geophys. Union, 583–590.

Lander, M., and G. J. Holland, 1993: On the interaction of tropical-cyclone scale vortices. I: Observations. *Quart. J. Roy. Meteor. Soc.,* **119,** 1347–1361.

Lemon, L. R., 1980: Severe thunderstorm radar identification techniques and warning criteria. NOAA Tech. Memo., NWS NSSFC-3, 60 pp. [NTIS PB 231409.]

Maddox, R. A., L. R. Hoxit, and C. F. Chappell, 1980: A study of tornadic thunderstorm interactions with thermal boundaries. *Mon. Wea. Rev.,* **108,** 322–336.

Miller, R. C., 1972: Notes on analysis and severe-storm forecasting procedures of the Air Force Global Weather Central. Air Weather Service Tech. Rept. 200 (Rev.), 190 pp. [Available from USAFETAC, Scott Air Force Base, IL 62225.]